Published in final edited form as:
Neuron. 2013 May 8; 78(3): 469–482. doi:10.1016/j.neuron.2013.03.005.

Three Mechanisms Assemble Central Nervous System Nodes of Ranvier

Keiichiro Susuki[1,8], **Kae-Jiun Chang**[2,8], **Daniel R. Zollinger**[1], **Yanhong Liu**[1], **Yasuhiro Ogawa**[1,9], **Yael Eshed-Eisenbach**[3], **María T. Dours-Zimmermann**[4], **Juan A. Oses-Prieto**[5], **Alma L. Burlingame**[5], **Constanze I. Seidenbecher**[6], **Dieter R. Zimmermann**[4], **Toshitaka Oohashi**[7], **Elior Peles**[3], and **Matthew N. Rasband**[1,2,*]

[1]Department of Neuroscience [2]Program in Developmental Biology Baylor College of Medicine, Houston, TX 77030, USA [3]Department of Molecular Cell Biology, Weizmann Institute of Science, Rehovot 76100, Israel [4]Institute of Surgical Pathology, University Hospital Zü rich, Zü rich CH-8091, Switzerland [5]Department of Pharmaceutical Chemistry, University of California San Francisco, San Francisco, CA 94158, USA [6]Leibniz Institute for Neurobiology, Magdeburg 39118, Germany [7]Department of Molecular Biology and Biochemistry, Okayama University Graduate School of Medicine, Dentistry and Pharmaceutical Sciences, Okayama 700-8558, Japan

Summary

Rapid action potential propagation in myelinated axons requires Na^+ channel clustering at nodes of Ranvier. However, the mechanism of clustering at CNS nodes remains poorly understood. Here, we show that the assembly of nodes of Ranvier in the CNS involves three mechanisms: a glia-derived extracellular matrix (ECM) complex containing proteoglycans and adhesion molecules that cluster NF186, paranodal axoglial junctions that function as barriers to restrict the position of nodal proteins, and axonal cytoskeletal scaffolds (CSs) that stabilize nodal Na^+ channels. We show that while mice with a single disrupted mechanism had mostly normal nodes, disruptions of the ECM and paranodal barrier, the ECM and CS, or the paranodal barrier and CS all lead to juvenile lethality, profound motor dysfunction, and significantly reduced Na^+ channel clustering. Our results demonstrate that ECM, paranodal, and axonal cytoskeletal mechanisms ensure robust CNS nodal Na^+ channel clustering.

Introduction

In myelinated nerve fibers, rapid action potential (AP) conduction depends on high densities of voltage-gated Na^+ channels clustered at regularly spaced sites called nodes of Ranvier. These nodes contain ion channels and cell adhesion molecules (e.g., neurofascin-186 [NF186]) that are linked to the axonal cytoskeleton by the scaffolding proteins ankyrinG (ankG) and βIV spectrin (Salzer, 2003). Together with myelin, clustered nodal proteins are responsible for the regeneration and rapid propagation of APs.

Node assembly depends on neuron-glia interactions between axons and oligodendrocytes in the CNS, and axons and Schwann cells in the peripheral nervous system (PNS) (Schafer and Rasband, 2006). These neuron-glia interactions require NF, since animals lacking NF fail to

*Correspondence: rasband@bcm.edu.
[8]These authors contributed equally to this work
[9]Present address: Department of Pharmacology, Meiji Pharmaceutical University, Tokyo 204-8588, Japan

Supplemental Information: Supplemental Information includes four figures, one table, three movies, and Supplemental Experimental Procedures and can be found with this article online at http://dx.doi.org/10.1016/j.neuron.2013.03.005.

cluster Na^+ channels or ankG (Sherman et al., 2005). In the PNS, during myelination the proteins gliomedin and NrCAM cluster axonal NF186 at the ends of the nascent myelin sheath (Eshed et al., 2005; Feinberg et al., 2010). Clustered NF186 then functions as an attachment site for ankG and the subsequent recruitment of Na^+ channels and βIV spectrin (Davis and Bennett, 1994; Gasser et al., 2012; Sherman et al., 2005; Yang et al., 2007). Little is known about the molecular mechanisms of CNS node formation, which must be different from PNS mechanisms because gliomedin is not found at CNS nodes (Eshed et al., 2005).

Three potential mechanisms have been proposed to operate during the assembly of nodes in the CNS: (1) clustering of NF186 by glia-derived ligands, (2) restriction of nodal proteins at the forming nodal gap by the paranodal axoglial junctions, and (3) stabilization of Na^+ channels by axonal cytoskeletal scaffolds (CSs; Susuki and Rasband, 2008). However, the specific contribution of these mechanisms, as well as their ability to compensate for each other, is unknown. Potential glial ligands that may cluster NF186 include the chondroitin sulfate proteoglycans brevican (Bcan) and versican (Vcan), since they are enriched in the extracellular matrix (ECM) surrounding CNS nodes (Dours-Zimmermann et al., 2009; Hedstrom et al., 2007; Oohashi et al., 2002). In support of this notion, Bcan was shown to bind NF186 (Hedstrom et al., 2007). However, mice lacking Bcan or Vcan have normal nodes (Bekku et al., 2009; Dours-Zimmermann et al., 2009), questioning their role in CNS node assembly. Alternatively, the paranodal axoglial junctions flanking nodes have been proposed to function as lateral diffusion barriers that restrict the position of nodal proteins in the axon (Pedraza et al., 2001; Rasband et al., 1999). Although there is strong experimental support for a paranodal barrier-like mechanism (Feinberg et al., 2010; Zonta et al., 2008), the idea remains controversial since disruption of paranodal junctions (PJs) alone causes only mild perturbations to Na^+ channel clustering (Bhat et al., 2001; Pillai et al., 2009; Thaxton et al., 2011). Finally, Na^+ channel binding to the CS ankG is both necessary and sufficient for channel clustering (Gasser et al., 2012). However, mice lacking nodal βIV spectrin, which links ankG and Na^+ channels to the actin cytoskeleton, have relatively normal CNS nodes (Komada and Soriano, 2002; Yang et al., 2004).

How can these differences and apparent contradictions be explained? One possibility is that these several mechanisms normally work together but can also function independently and compensate for one another. Here, we report that CNS nodes of Ranvier are assembled by three distinct mechanisms: (1) clustering of NF186 by a glia-derived ECM, (2) restriction of nodal protein mobility by paranodal axoglial barriers, and (3) stabilization of Na^+ channels by axonal CSs. Furthermore, we show that these mechanisms are complementary, since disruptions of either the ECM and paranodal barrier, the ECM and CSs, or the paranodal barrier and CSs in mice all cause significantly impaired node formation. Our results reveal multiple, overlapping mechanisms that together assemble CNS nodes of Ranvier.

Results

NF186 Can Be Localized to CNS Nodes through Extracellular or Cytoplasmic Interactions

Clustering of NF186 is sufficient to initiate clustering of ankG, Na^+ channels, and βIV spectrin (Eshed et al., 2007; Zonta et al., 2008). To determine if cytoplasmic and/or extracellular interactions cluster NF186 at CNS nodes of Ranvier, we constructed wild-type (WT) and truncated NF186-GFP fusion proteins (Figure 1A) and expressed them in cortical layer II/III neurons by in utero electroporation. We examined nodes in the corpus callosum of electroporated mice at postnatal day 28 (P28), because the axons of the transfected neurons project through the corpus callosum and many are myelinated by P28. We found that both full-length NF186 (NFfull-GFP) and NF186 lacking its cytoplasmic domain (NFΔCD-GFP) were strongly clustered at nodes, indicating that extracellular interactions

are sufficient for nodal clustering of NF186 (Figure 1B). Similarly to NFfull-GFP and NFΔCD-GFP proteins, NF lacking its extracellular domain (NFΔED-GFP) was also enriched at nodes of Ranvier (Figure 1B), indicating that interactions with the axonal cytoskeleton are also sufficient for NF clustering at nodes. However, consistent with one previous report (Dzhashiashvili et al., 2007), loss of the extracellular domain impaired the removal of the truncated protein from paranodal and internodal regions covered by the myelin sheath. To further characterize the cytoplasmic interaction necessary for nodal NF186 clustering, we deleted the five amino acids (FIGQY) responsible for ankG-binding (NFΔEΔF-GFP; Garver et al., 1997). In the absence of an extracellular domain, this deletion blocked NF186 enrichment at CNS nodes (Figure 1B). Similarly, a control transmembrane protein (CD4-GFP) showed no significant accumulation at nodes (Figure 1B). Quantification of the ratio of node/paranode GFP fluorescence intensity showed that NF186full-GFP, NFΔED-GFP, and NFΔCD-GFP were significantly more enriched at nodes than CD4-GFP (Figure 1C), although the ratio of nodal/paranodal enrichment in the NFΔED-GFP construct was dramatically reduced due to its failure to be removed from paranodal regions. We conclude that both extracellular and cytoplasmic interactions are sufficient to cluster NF186 at CNS nodes.

Extracellular Interactions: The “Core” CNS Nodal ECM

What extracellular molecules and interactions could be responsible for nodal clustering of NF186? Several ECM proteins have been reported at CNS nodes, and most of them are expressed by oligodendrocytes or their precursors (Cahoy et al., 2008; Zimmermann and Dours-Zimmermann, 2008). Therefore, the oligodendrocyte-derived factors that have been proposed to cluster Na^+ channels in CNS axons (Kaplan et al., 1997) could be the nodal ECM proteins and work through NF186. Consistent with this idea, the nodal ECM proteins Bcan and tenascin-R have been reported to interact with NF186 (Hedstrom et al., 2007; Volkmer et al., 1998). Nodal clustering of the ECM molecules phosphacan, tenascin-R, and neurocan (Ncan) depends on the proteoglycan Vcan and/or the proteoglycan Bcan (Figure 2A; Bekku and Oohashi, 2010; Bekku et al., 2009; Dours-Zimmermann et al., 2009). In addition, the hyaluronan-binding, brain-specific link protein Bral1 also colocalizes with Bcan and Vcan in the nodal ECM (Figure 2A; Oohashi et al., 2002). To identify the core components of the CNS nodal ECM and their interdependence for nodal localization, we examined adult KO mice lacking Bcan ($Bcan^{-/-}$), Vcan ($Vcan^{-/-}$), both Bcan and Vcan ($Bc^{-/-}$ $Vc^{-/-}$), or Bral1 ($Bral1^{-/-}$; Figure 2A). Whereas Bcan and Vcan do not depend on each other for nodal clustering, in a subset of CNS nodes Bral1 localization depends on Bcan and Vcan. We found that 97% of WT nodes in the adult mouse spinal cord were Bral1 positive, but only 94%, 57%, and 39% of spinal cord nodes were labeled by Bral1 antibodies in $Bcan^{-/-}$, $Vcan^{-/-}$, and $Bc^{-/-}$ $Vc^{-/-}$ mice, respectively. In adult $Bral1^{-/-}$ tissues, Bcan, Vcan, and Ncan were not found at nodes (Figure 2A; Bekku and Oohashi, 2010; Bekku et al., 2010). However, Bcan and Vcan were detected at CNS nodes during early development (Figure S1A available online), suggesting that Bral1 may function to stabilize nodal ECM components rather than promote their initial assembly. Thus, among the six previously described nodal ECM proteins, our results suggest that Bcan, Vcan, and Bral1 function together as core ECM molecules surrounding CNS nodes.

In addition to the ECM molecules described above, we also found that the extracellular domain of NrCAM, a cell adhesion molecule related to NF186, is secreted and incorporated into the CNS nodal ECM (Figures 2A and S1B–S1H). Importantly, the nodal localization of NrCAM was not affected by loss of Bcan, Vcan, or Bral1, and vice versa (Figure 2A). Thus, extracellular NrCAM is a core component of the nodal ECM, but not of the nodal proteoglycan-based ECM.

Core CNS Nodal ECM Components Interact with NF186 and Induce Node-like Clustering

To further define the molecular interactions between the core ECM components and NF186 or other axonal nodal membrane proteins, we constructed core nodal ECM-Fc fusion proteins and applied them to COS-7 cells expressing known nodal membrane proteins (Figure 2B; Table S1). We found specific interactions between NF186 and Bral1, NrCAM, and the C-terminal G3 domains of Bcan and Vcan (Figure 2B; Table S1). Pull-down experiments using the extracellular domain of NF186 (HA-NF186) further confirmed the interaction between NF186 and Bcan, Vcan, and Bral1 (Figure 2C). We previously showed that silencing the expression of NF186 in neurons blocked the clustering of Bcan at axon initial segments (AIS), an axonal domain that has a molecular organization similar to that of nodes (Hedstrom et al., 2007; Rasband, 2010). Similarly, Vcan is enriched at the AIS of neurons in vivo and in vitro, and loss of NF186 blocked its clustering at the AIS (Figures S1I and S1J). Thus, the CNS nodal ECM proteins Bcan, Vcan, Bral1, and NrCAM interact with NF186.

We next determined the interactions between the core ECM proteins themselves. Using cell-surface binding assays (Table S1), we found that NrCAM did not interact with other ECM molecules, consistent with the idea that nodal localization of secreted NrCAM is unrelated to the proteoglycan complexes (Figure 2A) and likely depends onbindingtoNF186. Finally, using Flag-tagged Bral1 (Flag-Bral1) and Fc fusion proteins, we observed strong interactions between Bral1 and the G1 domains of Bcan and Vcan (Figure 2D). Previous studies of the cartilage link protein Crtl1 (also known as HAPLN1), a paralog of Bral1, revealed that it interacts with the G1 domain of aggrecan, a chondroitin sulfate proteoglycan related to Vcan and Bcan, and stabilizes its interaction with hyaluronan by forming a ternary complex (Yamaguchi, 2000). Together, these results suggest that Bral1, Bcan, and Vcan stabilize each other's nodal localization by forming ternary complexes with hyaluronan surrounding nodes of Ranvier (Girard et al., 1992; LeBaron et al., 1992; Oohashi et al., 2002).

To begin to determine whether the core nodal ECM molecules participate in CNS node formation, we tested whether addition of ECM-Fc fusion proteins to cultured neurons in vitro was sufficient to induce formation of node-like clusters in the absence of glia. We incubated BcanG3-Fc and NrCAM-Fc with dorsal root ganglion (DRG) neurons transfected with HA-NF186, and found coclustering of Bcan or NrCAM and NF186 along axons (Figure 2E). Furthermore, the interaction between BcanG3-Fc and NF186 along axons could recruit ankG to these node-like clusters (Figure S1K).

PJ Formation Precedes Clustering of Nodal ECM and Axonal Proteins during CNS Node Development

In the PNS, gliomedin initiates node assembly at the edges of myelinating Schwann cells by binding to and clustering NF186 (Eshed et al., 2005). By analogy, if ECM protein-mediated clustering of NF186 initiates CNS node formation, then the assembly of the CNS nodal ECM must be temporally correlated with the clustering of NF186. To test this, we immunostained myelinating optic nerve axons from P10 through adulthood with antibodies against the nodal axonal proteins NF186 and βIV spectrin; the nodal ECM components Bcan, Vcan, and Bral1; and the PJ protein Caspr (Figures 3A–3E). We labeled optic nerve axons with antibodies against the PJ protein Caspr because in the CNS, PJs form before the clustering of Na^+ channels (Rasband et al., 1999). At P10, shortly after myelination begins, we found many immature Caspr-labeled single paranodes, nearly half of these lacking any flanking NF186 (Figure 3A). In contrast, <1% of NF186 clusters lacked flanking Caspr immunoreactivity. As myelination progressed (analyzed at P13 and P17), the majority of Caspr- and/or NF186-labeled sites had a mature appearance with NF186 flanked by Caspr

on both sides (Figure 3A). Immuno-staining with antibodies against βIV spectrin showed results similar to those obtained for NF186 (Figure 3B). Furthermore, when NF186 was detected at P10, it colocalized with βIV spectrin 93.5% of the time and in >98% of nodes at all later time points, indicating that βIV spectrin is recruited to developing nodes concurrently with NF186. Together, these data suggest that a single paranode forms at the end of a myelinating oligodendrocyte process (Rasband et al., 1999), followed by NF186 and βIV spectrin clustering adjacent to the PJ. In contrast to NF186 and βIV spectrin, ECM molecules accumulate at nascent nodes much later. At P10, 80% of sites showed single paranodes without enriched Bcan or Vcan (Figures 3C and 3D). When two paranodes were present, 100% had concentrated NF186 between them, but only half had Bcan or Vcan staining, and the immunoreactivity for these nodal proteoglycans was weaker than in adult optic nerves (Figures 3C and 3D). In parallel with development, Bcan and Vcan enrichment at nodes became more frequent in number and stronger in intensity. We also found that Bral1 could not be detected until P21 or later (Figure 3E), consistent with one previous report (Oohashi et al., 2002). Together, these results suggest that the nodal ECM is assembled after the formation of paranodes and the clustering of NF186, and that PJs may play a primary role in assembling CNS nodes of Ranvier.

A Genetic Strategy to Test Overlapping Mechanisms of CNS Node Formation

Our data suggest that the nodal ECM, PJs, and CSs normally work together but may also function independently and compensate for one another as redundant mechanisms to assemble CNS nodes. To directly test this idea and to determine the sufficiency of a single mechanism, we crossed mice with a disrupted nodal ECM mechanism (Bcan$^{-/-}$, Vcan$^{-/-}$, Bcan$^{-/-}$ Vcan$^{-/-}$, and Bral1$^{-/-}$; Bekku et al., 2010; Brakebusch et al., 2002; Dours-Zimmerman et al., 2009), mice with a disrupted PJ barrier mechanism (Caspr$^{-/-}$; Gollan et al., 2003), and mice with a disrupted CS mechanism (*SPNB4*$^{qv3J/qv3J}$, a βIV spectrin mutant, hereafter referred to as *qv3J*; Parkinson et al., 2001; Yang et al., 2004) to generate mutant mice with two of the three mechanisms simultaneously disrupted (Figure 3F). We did not analyze mutant mice lacking NrCAM and Caspr since NrCAM$^{-/-}$ Caspr$^{-/-}$ mice die at P8 due to the dramatic loss of PNS nodal Na^+ channel clustering and before node formation begins in the optic nerve (Feinberg et al., 2010).

Disruption of the Nodal ECM and PJs Causes Severe Neurological Phenotypes and a Decreased Number of Nodes

We confirmed the genotypes and loss of each targeted molecule in ECM+PJ mutants by immunostaining (Figure 4A) and PCR (not shown). In mutants with disrupted PJs, juxtaparanodal proteins (e.g., Kv1.2) are found at paranodes (Bhat et al., 2001; Poliak et al., 2001). In the ECM+PJ mutants, the simultaneous loss of one or two ECM molecules and PJs did not further disrupt other nodal ECM molecules (e.g., NrCAM) compared with the ECM mutants alone (Figure 4A). Nevertheless, in contrast to mice with a single disrupted mechanism, the double (Vcan$^{-/-}$ Caspr$^{-/-}$, Bcan$^{-/-}$ Caspr$^{-/-}$, or Bral1$^{-/-}$ Caspr$^{-/-}$) and triple (Bcan$^{-/-}$ Vcan$^{-/-}$ Caspr$^{-/-}$) ECM+PJ mutants began to show clear motor dysfunction during the second week after birth (Movie S1). Evaluation of motor performance using the accelerating rotarod showed significant motor deficits in Bcan$^{-/-}$ Caspr$^{-/-}$ and Vcan$^{-/-}$ Caspr$^{-/-}$ mutants at P18 (Figure 4B). A similar analysis could not be done in Bcan$^{-/-}$ Vcan$^{-/-}$ Caspr$^{-/-}$ triple mutants because they were too sick to perform the test. The symptoms were progressive and the ECM+PJ mutant mice died prematurely (Bcan$^{-/-}$ Caspr$^{-/-}$ mice at P22–P58, Vcan$^{-/-}$ Caspr$^{-/-}$ mice at P18–P23, and Bral1$^{-/-}$ Caspr$^{-/-}$ mice at P17–P31). The Bcan$^{-/-}$ Vcan$^{-/-}$ Caspr$^{-/-}$ mice died at P16 or were sacrificed at P18 for the analyses described below. Despite the severe motor deficits, we measured no significant slowing of the compound AP (CAP) conduction velocity in the optic nerves of P18 ECM+PJ mice compared with Caspr$^{-/-}$ mice (Figure S2E). We also observed no apparent disruption

of the molecular organization of individual CNS nodes in the optic nerves of the P18 ECM +PJ mutants (Figure 4C). However, we did observe a striking and significant reduction in the number of nodes of Ranvier. Compared with WT animals or animals with only a single mechanism disrupted (ECM or PJ), all of the ECM+PJ mutants had significantly reduced numbers of Na^+ channel clusters in their optic nerves (Figures 4D and 4E). This dramatic nodal reduction in ECM+PJ mutants is unlikely to be a consequence of impaired myelination or axon degeneration since compared with the single Caspr$^{-/-}$ mice, the reduction in the number of Na^+ channel clusters in ECM+PJ mutants (Figure 4E) was consistently greater than the change in the number of myelinated axons (Figures S2A and S2B). To further confirm the loss of nodes in ECM+PJ mutants and to more directly show that this is not a consequence of impaired myelination, we double labeled P18 spinal cords for Na^+ channels and claudin-11, a marker of the autotypic paranodal tight junction (Gow et al., 1999). For this analysis, nodes were defined by two adjacent paranodes labeled for claudin-11 (Figure 4F). Thus, only confirmed myelinated axons were counted in this analysis. In ECM+PJ mutants, the frequency of nodes with Na^+ channel clusters was dramatically reduced compared with WT, ECM, or PJ mutant mice (Figures 4F and 4G).

The reduction in Na^+ channel clustering at P18 could be due to a failure to cluster or to maintain nodal Na^+ channels. To distinguish between these possibilities, we examined Na^+ channel clustering in P12 optic nerves, a very early developmental time point when node formation is just beginning. We found that Na^+ channel clusters were significantly reduced in Bcan$^{-/-}$ Caspr$^{-/-}$ mouse optic nerves (Figure S2C), suggesting the initial assembly of nodes is impaired in ECM+PJ mutants. Furthermore, using double immunostaining for claudin-11 and Na^+ channels in the spinal cord, we found that the reduction of nodes with Na^+ channel clusters in Bcan$^{-/-}$ Caspr$^{-/-}$ mice was comparable between P12and P18 (Figure S2D). Together, these results suggest that there is no evolving loss of nodal Na^+ channel clusters in ECM+PJ mutants; rather, there is a developmental defect in their assembly.

In the PNS, we found no significant difference in the nodal Na^+ channel cluster density (Figure S2F) or nerve conduction velocity between PJ and ECM+PJ mutants (Figure S2G) since the ECM components that are disrupted in these animals are specific for CNS nodes. Together with this finding, the significant reduction in CNS nodal Na^+ channel clusters in ECM+PJ mutants compared with ECM or PJ mutants alone supports the conclusion that in the CNS, ECM and PJ barrier mechanisms work together to assemble nodes, but the remaining ECM and cytoskeletal interactions are only partially sufficient to form nodes.

Mutants with Disruption of the Nodal ECM and CS Have Severe Neurologic Phenotypes and Decreased Nodal Densities

Next, we crossed βIV spectrin mutant mice (*qv3J*) with Bcan$^{-/-}$ or Vcan$^{-/-}$ mice to disrupt the ECM and CS at the same time, but leaving the paranodes intact (ECM+CS mutants; Figure 3F). In these double mutants, the loss of Bcan did not affect the nodal localization of Vcan, and vice versa, indicating that the ECM disruption in these double mutants is only a partial disruption (Figure 5A). Nevertheless, the ECM+CS mutants began to show motor impairment during the second week after birth (Movie S2) and most of them died or had to be euthanized between 3 and 4 weeks of age. ECM+CS mutants showed significant motor deficits on the accelerating rotarod at P18 (Figure 5B). Despite the severe phenotypes of the ECM+CS mutants, we measured no apparent slowing of conduction in their optic nerves compared with *qv3J* mice (Figure S3C). Furthermore, we observed no major difference in the molecular architecture of individual nodes in ECM+CS mutants compared with WT or *qv3J* mice (Figure 5C; Vcan$^{-/-}$ *qv3J* double mutants not shown). However, in Bcan$^{-/-}$ *qv3J* optic nerves, the number of nodal Na^+ channel clusters was significantly reduced (Figures 5D and 5E), with no major difference in myelinated axons compared with single mutants (Figures S3A and S3B). Similarly, the frequency of nodes, defined by paranodal claudin-11

and labeled for Na^+ channels, was reduced in $Bcan^{-/-}$ *qv3J* spinal cords (Figures 5F and 5G). In $Vcan^{-/-}$ *qv3J* optic nerves, the reduction in node density compared with *qv3J* did not reach statistical significance (Figure 5E) despite a reduction in the number of myelinated axons (Figure S3B). However, in $Vcan^{-/-}$ *qv3J* spinal cords, the frequency of nodes with Na^+ channel clusters was reduced at P18 (Figure 5G; 68.2%, n = 2) compared with single mutants and WT, with no apparent evolving loss at P27 (65.3%, n = 2). As expected, no change was seen in the PNS nodal density (Figure S3D) or nerve conduction velocity (Figure S3E). Together, the severe motor impairment, juvenile lethality, and reduced number of Na^+ channel clusters in the ECM+CS mice support the conclusion that in the CNS the ECM and cytoskeletal mechanisms work together to facilitate CNS node formation. Furthermore, the preserved nodal molecular organization but fewer Na^+ channel clusters suggests that the intact paranodes and remaining ECM molecules are only partially sufficient to assemble CNS nodes.

Loss of PJs and CSs Causes Severe Neurologic Phenotypes and Remarkably Disorganized and Reduced Numbers of Nodes in the CNS

One limitation of our strategy to disrupt two nodal clustering mechanisms simultaneously was that for practical reasons, we were unable to completely remove all nodal ECM proteins in the ECM+PJ and ECM+CS mutants. Consequently, instead of a complete loss of nodes, the 30%–50% reduction in Na^+ channel clustering in ECM+PJ and ECM+CS mutants (Figures 4E and 5E) likely reflects a rescue of node formation by the remaining nodal ECM components together with one intact clustering mechanism (CS or PJ). Therefore, to completely disrupt two clustering mechanisms, we produced *qv3J* $Caspr^{-/-}$ mutants with disrupted cytoskeletal interactions and disrupted PJs (CS+PJ) but intact nodal ECM (Figure 3F). The *qv3J* $Caspr^{-/-}$ mutants began to show profound motor deficits (Movie S3) in the second week after birth. The phenotype of these mice was even more severe than that of the ECM+PJ or ECM+CS mutant mice, and most died at P17 or P18. Rotarod tests could not be performed on the *qv3J* $Caspr^{-/-}$ double mutants, because by P17 and P18 most of these animals were moribund. The most striking finding in these *qv3J* $Caspr^{-/-}$ (CS+PJ) mutants was the remarkable ~70% loss of Na^+ channel clusters in the P18 optic nerves compared with CS or PJ mutants alone (Figures 6A and 6B). Analysis of spinal cord nodes defined by claudin-11 immunostaining also showed a profound reduction in Na^+ channel clustering in *qv3J* $Caspr^{-/-}$ mice (Figures 6C and 6D). When Na^+ channel clusters were present, they were disorganized, very elongated, and often lacked flanking Kv1.2-containing K^+ channels, but these aberrant clusters still contained NF186 and ankG (Figure 6E). Consistent with the dramatic loss of Na^+ channel clusters and disrupted nodal organization, we measured a significant decrease in nerve conduction velocity in the *qv3J* $Caspr^{-/-}$ mice compared with *qv3J* or $Caspr^{-/-}$mice alone (Figure 6F). Myelination in *qv3J* $Caspr^{-/-}$ mice was comparable to that in $Caspr^{-/-}$ mice with no sign of axon degeneration (Figure S4). Together, these data demonstrate that both paranodal barrier and CS mechanisms play essential roles in the assembly of CNS nodes of Ranvier.

What mechanism accounts for the few clusters of Na^+ channels, NF186, and ankG that still formed in the *qv3J* $Caspr^{-/-}$ mice (Figures 6A, 6B, and 6E)? When we immunostained optic nerves from *qv3J* $Caspr^{-/-}$ mice, we found that as in WT mice, Na^+ channel clusters were associated with Bcan, Vcan, and NrCAM (Figure 6G), suggesting that these ECM molecules are sufficient to cluster Na^+ channels in the absence of cytoskeletal scaffolding and paranodal barrier mechanisms, and partially rescue node assembly.

Mutants with Disrupted PJs and Axonal Cytoskeletons Have Normal PNS Nodes

As described above, ECM+PJ and ECM+CS mutants had normal PNS nodes of Ranvier, since PNS nodes have a different nodal ECM (Figures S2 and S3). However, since *qv3J*

Caspr$^{-/-}$ mice lack CS+PJ mechanisms in both the CNS and PNS, they offer a unique opportunity to contrast the roles of each mechanism in CNS and PNS node formation. We confirmed that *qv3J* Caspr$^{-/-}$ PNS paranodes are disrupted and have Kv1.2 channels mislocalized in paranodal regions (Figure 7A). We also confirmed the loss of βIV spectrin from sciatic nerve nodes by using antibodies against βIV spectrin's N terminus (Figure 7A). Surprisingly, despite the severe disorganization of CNS nodes in *qv3J* Caspr$^{-/-}$ mice, the PNS nodes were preserved and indistinguishable from nodes in Caspr$^{-/-}$ mice (Figure 7A). Furthermore, despite the ~70% reduction in the number of Na^+ channel clusters in the CNS, we found no significant reduction in the nodal density in the sciatic nerve compared with CS or PJ mutants (Figure 7B). Finally, we found that the motor nerve conduction velocity in the sciatic nerves from *qv3J* Caspr$^{-/-}$– mice was not significantly different from that in Caspr$^{-/-}$ mice (Figure 7C). Thus, the PNS nodal ECM, but not the CNS nodal ECM, is sufficient to assemble a normal contingent of nodes of Ranvier. Furthermore, these results strongly suggest that PJ and cytoskeletal mechanisms are more important for nodal Na^+ channel clustering in the CNS than in the PNS.

Discussion

Clustered Na^+ channels at nodes of Ranvier dramatically increase the speed and significantly reduce the metabolic demands of AP conduction in myelinated axons. While much is known about the mechanisms of Na^+ channel clustering at nodes in the PNS and the molecules involved (Feinberg et al., 2010; Sherman et al., 2005), the proposed mechanisms for the CNS are controversial and remain poorly understood. Here, we identified the molecules and three mechanisms (Figure 6H) that contribute to Na^+ channel clustering at CNS nodes. The loss or disruption of nodes, as a consequence of disease or injury, impairs nervous system function. Therefore, therapeutic strategies aimed at repairing the nervous system require a detailed understanding of the mechanisms of node formation and the role that myelinating glia play in node assembly.

Mechanism 1: Interaction with the Nodal ECM

CNS nodes of Ranvier are surrounded by a complex ECM consisting of Bcan, Vcan, Ncan, phosphacan, tenascin-R, Bral1, and NrCAM. Among these ECM components, Bcan, Vcan, Bral1, and NrCAM comprise a core ECM and contribute to Na^+ channel clustering by binding to and stabilizing the cell adhesion molecule NF186. This conclusion is based on several observations: (1) NF186 lacking its cytoplasmic domain can cluster at CNS nodes, indicating that extracellular interactions with the ECM are sufficient for its nodal localization; (2) Bcan, Vcan, Bral1, and NrCAM bind directly to NF186; (3) nodal ECM components can promote node-like clusters of NF186 in vitro; (4) CNS nodes can assemble in association with the core ECM proteins in mutant mice lacking both PJs and CSs; and (5) mutant mice with a disrupted ECM and loss of PJs or disrupted ECM and loss of CSs have severe motor dysfunction and a significantly reduced number of Na^+ channel clusters compared with mutants lacking only a single mechanism.

Despite their importance, not all ECM components are equally represented at CNS nodes. For example, some normal adult nodes lack Bcan (Figure 3; Bekku et al., 2009). Consistent with this observation, mutants deficient for a single ECM component do not show apparent phenotypes or altered CNS nodes (Bekku et al., 2010; Brakebusch et al., 2002; Dours-Zimmermann et al., 2009). Our genetic analyses of double- and triple-knockout mice suggest that this may be explained by compensation by other ECM molecules, PJs, and CSs. Furthermore, the developmental delay in the enrichment of ECM proteins surrounding the CNS nodes suggests that under normal conditions they may play more important roles in stabilizing nodal proteins than in contributing to their initial assembly. However, in mutants with disrupted paranodes and/or CSs, we conclude that the nodal ECM contributes to initial

node formation. Although our experiments did not reveal a progressive loss of Na^+ channel clusters, our experiments were unable to determine whether ECM proteins contribute to stabilizing nodal Na^+ channel clusters for longer periods. It is interesting to note that many of these same ECM proteins have been reported to stabilize synapses and affect synaptic plasticity (Frischknecht et al., 2009). We speculate that nodal ECM proteins may contribute to the plasticity of node location and internodal length, which in turn could influence the timing of AP arrival in neural circuits (Seidl et al., 2010). In the PNS, the major Na^+ channel clustering mechanism is the interaction between the nodal ECM proteins gliomedin and NrCAM and their axonal receptor NF186 (Feinberg et al., 2010). This conclusion is further supported by our results showing that mutant mice lacking both paranodal and cytoskeletal mechanisms have normal Na^+ channel clustering in the PNS (Figure 7).

Mechanism 2: Paranodal Diffusion Barriers

PJs are formed by interactions between glial NF155 and the axonal cell adhesion molecules Caspr and contactin, although the exact details of these interactions remain unclear (Charles et al., 2002; Gollan et al., 2003). PJs function as lateral diffusion barriers to restrict the mobility of axolemmal membrane proteins between two growing myelin internodes (Bhat et al., 2001; Dupree et al., 1999; Feinberg et al., 2010; Poliak et al., 2001; Rasband et al., 1999; Rios et al., 2003; Zonta et al., 2008). The results presented here are consistent with this view and support amodel for node formation in which paranodal diffusion barriers are the primary mechanism of Na^+ channel clustering in the CNS. This interpretation is based on the observations that (1) during early development, PJs formed before clusters of NF186 or βIV spectrin appeared, and before ECM molecules accumulated at nodes; (2) double and triple mutants lacking PJs were always more severe than single knockouts; (3) CS+PJ mutants had profound loss of Na^+ channel clustering in the CNS; and (4) ECM+CS mutants had the best-preserved Na^+ channel clustering in the spinal cord, emphasizing that PJs have the ability to form CNS nodes of Ranvier and can compensate for the loss of the CS and ECM.

The idea that PJs constitute an independent mechanism for Na^+ channel clustering is controversial. Thaxton et al. (2011) reported that paranodes do not contribute to Na^+ channel clustering, since the loss ofneuronal NF186 alone blocked Na^+ channel clustering despite intact paranodes. In contrast, other studies showed that expression of glial NF155 in an NF-null mouse is sufficient to rescue PJs and Na^+ channel clustering in the CNS (Zonta et al., 2008). Furthermore, coculture of WT Schwann cells with NF-null DRG neurons is sufficient to induce clustering of Na^+ channels adjacent to paranodes (Feinberg et al., 2010). The data presented here do not resolve the issue of whether PJs first cluster NF186 and then ankG is clustered through its interaction with NF186, or PJs and the associated paranodal cytoskeleton are sufficient to cluster ankG without NF186. Nevertheless, they do resolve some of the controversy because the intact ECM-NF186 interaction alone (CS+PJ mutant) resulted in profound loss of Na^+ channel clustering. Taken together, these data support the view that paranodes play important roles in normal CNS node of Ranvier formation and that NF186-ECM interactions alone are insufficient to assemble a normal complement of nodes of Ranvier.

How do PJs function as a membrane diffusion barrier to limit the lateral diffusion of membrane proteins? One possibility is that the cytoskeletal molecules at PJs form a boundary that effectively “fences in” the nodal axonal cytoskeleton. Consistent with this idea, we recently showed that during development the distal axonal submembranous cytoskeleton, comprised of ankyrinB, αII spectrin, and βII spectrin, defines a boundary that limits ankG to the proximal axon, resulting in the clustering of ankG, Na^+ channels, NF186, and βIV spectrin at AIS (Galiano et al., 2012). The submembranous axonal cytoskeleton found at PJs is similar in composition (Ogawa et al., 2006) and may confine ankG and βIV spectrin between the paranodes. Future studies of mutant mice lacking these CSs will help to

test this possibility, although single knockouts are unlikely to result in disrupted nodes given the availability of the compensatory ECM and CS mechanisms. The PJ may also function as a barrier at the level of the plasma membrane due to the unique lipid environment found at paranodes (Dupree and Pomicter, 2010; Schafer et al., 2004). In this view, axonal membrane proteins are restricted to their unique domains not only through protein-protein interactions with cytoskeletal and extracellular binding partners but also as a consequence of the lipid domains that they prefer or from which they are excluded.

Mechanism 3: CSs

The ankyrin-binding motif in Na^+ channels is both necessary and sufficient for Na^+ channel localization to nodes (Gasser et al., 2012), and βIV spectrin's clustering at CNS and PNS nodes also depends on its ankyrin-binding domain (Yang et al., 2007). Furthermore, in vitro small hairpin RNA (shRNA)-mediated knockdown of ankG in myelinating DRG-Schwann cell cocultures blocked Na^+ channel clustering at gaps in the myelin sheath (Dzhashiashvili et al., 2007). Based on its similarity to other ankyrin-containing protein complexes, ankG is thought to cluster membrane proteins and connect them to the actin cytoskeleton through βIV spectrin (Bennett and Baines, 2001). Together, these studies support the conclusion that an ankG-βIV spectrin complex plays essential roles in node of Ranvier formation and stabilization. Our results support and extend this concept since 1) a GFP-tagged NF construct lacking the extracellular domain clustered at CNS nodes, (2) deletion of the extracellular domain and ankG-binding motif blocked NF clustering at CNS nodes, (3) ECM +CS and CS+PJ mutants had significantly fewer CNS nodes of Ranvier than ECM or PJ mutants alone, and (4) ECM+PJ mutants had ~50%-70% of the normal complement of CNS nodes in the optic nerve, suggesting that the preserved cytoskeletal interactions could partially compensate for the disrupted ECM and loss of PJs. Thus, a cytoskeletal mechanism involving an ankG-βIV spectrin protein complex and the actin cytoskeleton contributes to node formation.

A Model for CNS Node Formation

Although the results presented here are consistent with a model in which multiple mechanisms normally contribute to ankG and Na^+ channel clustering along myelinated axons, our analyses also suggest that they are not equally redundant. During development of CNS nodes, we found that PJs formed before the nodal clustering of ECM proteins or CSs. Furthermore, the severity of the double- and triple-mutant phenotypes varied depending on the mechanisms that were disrupted. In general, the most severe double and triple mutants were those that lacked PJs. For example, on the $Vcan^{-/-}$ background, loss of paranodes reduced Na^+ channel clustering (only 36% of nodes had Na^+ channel clusters in the spinal cords of $Vcan^{-/-}$ $Caspr^{-/-}$ double mutants) more than loss of the cytoskeleton did (68% had Na^+ channel clusters in the $Vcan^{-/-}$ *qv3J* double mutants). Furthermore, the ECM seems to be less important than paranodes in normal development since the nodal ECM assembles after paranode/node formation (Figure 3). Thus, we propose that PJs play the primary role in CNS node formation (Figure 6H). In contrast, in the PNS the ECM is the primary mechanism for node assembly (Figure 7D) since (1) clustering of NF186 and gliomedin occurs before the formation of paranodes (Eshed et al., 2005; Schafer et al., 2006), (2) double-mutant mice with disrupted PNS ECM and PJs (ECM+PJ; $gliomedin^{-/-}$ $Caspr^{-/-}$ and $NrCAM^{-/-}$ $Caspr^{-/-}$) have remarkably disorganized and reduced Na^+ channel clusters (Feinberg et al., 2010), and (3) the analysis of CS+PJ mutant mice in this study showed intact PNS nodes.

In summary, our data support a model in which neuron-glia interactions first cluster ankG and NF186 adjacent to forming paranodes. Next, the ankG-Na^+ channel nodal complex is stabilized through interactions between βIV spectrin and the actin cytoskeleton, and through

NF186 and the nodal ECM. We conclude that in CS mutants, nodes remain intact since PJs restrict nodal proteins and NF186-ECM interactions stabilize the nodal protein complex. In ECM mutants, nodes form since PJs restrict nodal proteins, and βIV spectrin interactions with the actin-based cytoskeleton stabilize the nodal protein complex. In PJ mutants, nodes still form since NF186 can interact with the ECM, recruit ankG and Na^+ channels, and be further stabilized through βIV spectrin interactions with the actin cytoskeleton. The existence of multiple mechanisms that contribute to CNS node of Ranvier formation ensures their proper assembly and highlights the importance of nodes for efficient nervous system function.

Experimental Procedures

Animals

Animals were housed at the Center for Laboratory Animal Care at Baylor College of Medicine. All procedures were approved by the Institutional Animal Care and Use Committee at Baylor College of Medicine and conform to the US Public Health Service Policy on Human Care and Use of Laboratory Animals. The following single-mutant mice were produced as described previously: $Bcan^{-/-}$ (C57BL/6) (Brakebusch et al., 2002); $Vcan^{-/-}$(C57BL/6J) (Dours-Zimmermann et al., 2009); $Bral1^{-/-}$ (ICR)(Bekku et al., 2010); $Caspr^{-/-}$ (ICR) (Gollan et al., 2003); and *qv3J* (C57BL/6J) (Parkinson et al., 2001).

Antibodies

A detailed list of the antibodies used here can be found in the Supplemental Experimental Procedures.

DNA Constructs

A description of the complementary DNAs (cDNAs) and shRNAs used here can be found in the Supplemental Experimental Procedures.

Preparation of Media Containing Secreted Proteins

The HA-NF186ECD, Flag-Bral1, and various Fc constructs were transfected into COS-7 cells and the media were changed to virus-production serumfree medium (VP-SFM) supplemented with 2× GlutaMAX-I 1 day after transfection; harvested 2, 3, or 4 days after transfection; and neutralized with Tris-HCl (pH 8.0). The media with Fc fusions were concentrated 12- to 15-fold and buffer-exchanged to Neurobasal (Life Technologies). Small-scale purification of Fc, BcanG3-Fc, VcanG3-Fc, and Bral1-Fc was done by incubating the unconcentrated or concentrated media containing 0.05% [v/v] Triton X-100 with 20 ml of protein A agarose beads (Thermo Scientific) overnight at 4°C, washing the beads with 1 ml of ice-cold PBST (149.8 mM NaCl, 10.4 mM NaPi [pH 7.2], 0.05% Triton X-100) once and PBS (149.8 mM NaCl, 10.4 mM NaPi [pH 7.2]) twice, eluting with 100 μl of 80 mM glycine-HCl (pH 2.5) at room temperature (RT) and neutralizing with 10 μl of 1 M HEPES-NaOH (pH 8.0).

COS-7 Cell-Surface Binding and DRG Neuron-Clustering Assays

The concentrated media or eluates of small-scale purification containing Fc fusions were preclustered with fluorescein isothiocyanate (FITC) or Texas Red-conjugated anti-human Fcγ at 1:200 on icefor30min. COS-7 cells grown on glass coverslips and transfected with HA-NF186, contactin, Navβ1-V5-His, Navβ2-V5-His, Navβ4-EGFP, or HA-NrCAM were incubated with preclustered Fc fusions at RT for 30 min, washed with ice-cold PBS three times, fixed with 4% paraformaldehyde in 0.1 M PB (19 mM NaH_2PO_4, 81 mM Na_2HPO_4, pH7.2) at 4°C for 20 min, and immunostained as described previously (Hedstrom et al.,

2007). Purified DRG neuron culture was prepared as described previously (Susuki et al., 2011). At 10–12 days in vitro (DIV), the DRG neurons grown on coverslips were transfected with HA-NF186 by using Lipofectamine LTX and Plus reagent (both from Life Technologies) and washed twice with Neurobasal. Two days later, the neurons were incubated with the preclustered Fc fusions at RT for 30 min, cultured for 2 more days in the original medium (Neurobasal supplemented with 1 × GlutaMAX-I, 1 × B-27 Supplement [Life Technologies], and 100 ng/ml recombinant rat β-NGF [R&D Systems]), fixed, and immunostained.

Pull-Down Assays

For pull-down of HA-NF186ECD, the unconcentrated or concentrated media of Fc fusions containing 0.01% Triton X-100 were incubated with 10–20 μl of protein A agarose beads for 2–6 hr at 4°C. The beads were washed with ice-cold modified NET-2 buffer (150 mM NaCl, 10 mM Tris-HCl pH 7.5, 0.01% Triton X-100) three times and incubated with the media of HA-NF186ECD supplemented with 0.01% Triton X-100 overnight at 4°C. The beads were then washed with the ice-cold modified NET-2 buffer four times and the precipitated material was analyzed by western blotting. For pull-down of Flag-Bral1, the media of Fc fusions containing 0.05% Triton X-100 were incubated with 20 ml of protein A agarose beads for 2 hr at 4°C. The beads were washed with ice-cold PBST three times and incubated with the media of Flag-Bral1 supplemented with 0.05% Triton X-100 overnight at 4°C. The beads were then washed with ice-cold PBST four times and analyzed by western blotting.

Hippocampal Neuron Culture and shRNA Knockdown

Details about the primary hippocampal neuron cultures and knockdown of proteins by shRNA can be found in the Supplemental Experimental Procedures.

In Utero Electroporation

In utero electroporation of truncated NF186 or CD4 plasmids was performed in E14 mouse embryos as described previously (Saito, 2006). Injected mice were born and allowed to develop 28 days before being killed. Brains were fixed, sectioned, and stained as described previously (Schafer et al., 2004).

Immunofluorescence Studies

Details of the immunostaining procedures can be found in the Supplemental Experimental Procedures.

Rotarod

An accelerating rotarod was used to analyze motor coordination as described elsewhere (Chang et al., 2010).

Electrophysiology

CAP recordings in optic nerve and sciatic nerve were performed as described elsewhere (Rasband et al., 1999; Susuki et al., 2007).

Transmission Electron Microscopy

Electron microscopy was performed as described before (Chang et al., 2010). The sectioning and electron microscopy were performed in the Baylor College of Medicine Integrated Microscopy Core.

Statistical Analysis

Statistical significance was determined using a Kruskal-Wallis test. To further analyze which experimental group differed from the relevant control group, planned comparisons were done by Mann-Whitney's test according to Bonferroni correction. For the analyses of double mutants, comparison was performed among four groups: WT, mutant 1, mutant 2, and double mutants of 1 and 2. Data are shown in a box-and-whisker plot (median: a line across the box; 25th and 75th percentiles: lower and upper box edges, respectively; minimum and maximum: the values below and above the box, respectively).

Supplementary Material

Refer to Web version on PubMed Central for supplementary material.

Acknowledgments

The authors thank Debra Townley (Integrated Microscopy Core, Baylor College of Medicine) and Marlesa Godoy (Department of Neuroscience, Baylor College of Medicine) for technical assistance. This work was supported by grants from the NIH (NS069688 and NS044916 to M.N.R., and NS50220 to E.P.); the Dr. Miriam and Sheldon Adelson Medical Research Foundation; the Ministry of Education, Culture, Sports Science, and Technology (MEXT) of Japan (24107516 to T.O.); and the U.S.-Israel Binational Science Foundation. E.P. is the Incumbent of the Hanna Hertz Professorial Chair for Multiple Sclerosis and Neuroscience.

References

Bekku Y, Oohashi T. Neurocan contributes to the molecular heterogeneity of the perinodal ECM. Arch Histol Cytol. 2010; 73:95–102. [PubMed: 21566336]

Bekku Y, Rauch U, Ninomiya Y, Oohashi T. Brevican distinctively assembles extracellular components at the large diameter nodes of Ranvier in the CNS. J Neurochem. 2009; 108:1266–1276. [PubMed: 19141078]

Bekku Y, Vargová L, Goto Y, Vorísek I, Dmytrenko L, Narasaki M, Ohtsuka A, Fässler R, Ninomiya Y, Syková E, Oohashi T. Bral1: its role in diffusion barrier formation and conduction velocity in the CNS. J Neurosci. 2010; 30:3113–3123. [PubMed: 20181608]

Bennett V, Baines AJ. Spectrin and ankyrin-based pathways: metazoan inventions for integrating cells into tissues. Physiol Rev. 2001; 81:1353–1392. [PubMed: 11427698]

Bhat MA, Rios JC, Lu Y, Garcia-Fresco GP, Ching W, St Martin M, Li J, Einheber S, Chesler M, Rosenbluth J, et al. Axon-glia interactions and the domain organization of myelinated axons requires neurexin IV/Caspr/Paranodin. Neuron. 2001; 30:369–383. [PubMed: 11395000]

Brakebusch C, Seidenbecher CI, Asztely F, Rauch U, Matthies H, Meyer H, Krug M, Bo¨ckers TM, Zhou X, Kreutz MR, et al. Brevican-deficient mice display impaired hippocampal CA1 long-term potentiation but show no obvious deficits inlearning and memory. Mol Cell Biol. 2002; 22:7417–7427. [PubMed: 12370289]

Cahoy JD, Emery B, Kaushal A, Foo LC, Zamanian JL, Christopherson KS, Xing Y, Lubischer JL, Krieg PA, Krupenko SA, et al. A transcriptome database for astrocytes, neurons, and oligodendrocytes: a new resource for understanding brain development and function. J Neurosci. 2008; 28:264–278. [PubMed: 18171944]

Chang KJ, Susuki K, Dours-Zimmermann MT, Zimmermann DR, Rasband MN. Oligodendrocyte myelin glycoprotein does not influence node of ranvier structure or assembly. J Neurosci. 2010; 30:14476–14481. [PubMed: 20980605]

Charles P, Tait S, Faivre-Sarrailh C, Barbin G, Gunn-Moore F, Denisenko-Nehrbass N, Guennoc AM, Girault JA, Brophy PJ, Lubetzki C. Neurofascin is a glial receptor for the paranodin/Caspr-contactin axonal complex at the axoglial junction. Curr Biol. 2002; 12:217–220. [PubMed: 11839274]

Davis JQ, Bennett V. Ankyrin binding activity shared by the neurofascin/L1/NrCAM family of nervous system cell adhesion molecules. J Biol Chem. 1994; 269:27163–27166. [PubMed: 7961622]

Dours-Zimmermann MT, Maurer K, Rauch U, Stoffel W, Fässler R, Zimmermann DR. Versican V2 assembles the extracellular matrix surrounding the nodes of Ranvier in the CNS. J Neurosci. 2009; 29:7731–7742. [PubMed: 19535585]

Dupree JL, Pomicter AD. Myelin, DIGs, and membrane rafts in the central nervous system. Prostaglandins Other Lipid Mediat. 2010; 91:118–129. [PubMed: 19379822]

Dupree JL, Girault JA, Popko B. Axo-glial interactions regulate the localization of axonal paranodal proteins. J Cell Biol. 1999; 147:1145–1152. [PubMed: 10601330]

Dzhashiashvili Y, Zhang Y, Galinska J, Lam I, Grumet M, Salzer JL. Nodes of Ranvier and axon initial segments are ankyrin G-dependent domains that assemble by distinct mechanisms. J Cell Biol. 2007; 177:857–870. [PubMed: 17548513]

Eshed Y, Feinberg K, Carey DJ, Peles E. Secreted gliomedin is a perinodal matrix component of peripheral nerves. J Cell Biol. 2007; 177:551–562. [PubMed: 17485493]

Eshed Y, Feinberg K, Poliak S, Sabanay H, Sarig-Nadir O, Spiegel I, Bermingham JR Jr, Peles E. Gliomedin mediates Schwann cell-axon interaction and the molecular assembly of the nodes of Ranvier. Neuron. 2005; 47:215–229. [PubMed: 16039564]

Feinberg K, Eshed-Eisenbach Y, Frechter S, Amor V, Salomon D, Sabanay H, Dupree JL, Grumet M, Brophy PJ, Shrager P, Peles E. A glial signal consisting of gliomedin and NrCAM clusters axonal Na+ channels during the formation of nodes of Ranvier. Neuron. 2010; 65:490–502. [PubMed: 20188654]

Frischknecht R, Heine M, Perrais D, Seidenbecher CI, Choquet D, Gundelfinger ED. Brain extracellular matrix affects AMPA receptor lateral mobility and short-term synaptic plasticity. Nat Neurosci. 2009; 12:897–904. [PubMed: 19483686]

Galiano MR, Jha S, Ho TS, Zhang C, Ogawa Y, Chang KJ, Stankewich MC, Mohler PJ, Rasband MN. A distal axonal cytoskeleton forms an intra-axonal boundary that controls axon initial segment assembly. Cell. 2012; 149:1125–1139. [PubMed: 22632975]

Garver TD, Ren Q, Tuvia S, Bennett V. Tyrosine phosphorylation at a site highly conserved in the L1 family of cell adhesion molecules abolishes ankyrin binding and increases lateral mobility of neurofascin. J Cell Biol. 1997; 137:703–714. [PubMed: 9151675]

Gasser A, Ho TSY, Cheng X, Chang KJ, Waxman SG, Rasband MN, Dib-Hajj SD. An ankyrinG-binding motif is necessary and sufficient for targeting Nav1.6 sodium channels to axon initial segments and nodes of Ranvier. J Neurosci. 2012; 32:7232–7243. [PubMed: 22623668]

Girard N, Courel MN, Delpech A, Brückner G, Delpech B. Staining of hyaluronan in rat cerebellum with a hyaluronectin-antihyaluronectin immune complex. Histochem J. 1992; 24:21–24. [PubMed: 1372596]

Gollan L, Salomon D, Salzer JL, Peles E. Caspr regulates the processing of contactin and inhibits its binding to neurofascin. J Cell Biol. 2003; 163:1213–1218. [PubMed: 14676309]

Gow A, Southwood CM, Li JS, Pariali M, Riordan GP, Brodie SE, Danias J, Bronstein JM, Kachar B, Lazzarini RA. CNS myelin and sertoli cell tight junction strands are absent in Osp/claudin-11 null mice. Cell. 1999; 99:649–659. [PubMed: 10612400]

Hedstrom KL, Xu X, Ogawa Y, Frischknecht R, Seidenbecher CI, Shrager P, Rasband MN. Neurofascin assembles a specialized extracellular matrix at the axon initial segment. J Cell Biol. 2007; 178:875–886. [PubMed: 17709431]

Kaplan MR, Meyer-Franke A, Lambert S, Bennett V, Duncan ID, Levinson SR, Barres BA. Induction ofsodium channel clustering by oligodendrocytes. Nature. 1997; 386:724–728. [PubMed: 9109490]

Komada M, Soriano P. [Beta]IV-spectrin regulates sodium channel clustering through ankyrin-Gat axon initial segments and nodes of Ranvier. J Cell Biol. 2002; 156:337–348. [PubMed: 11807096]

LeBaron RG, Zimmermann DR, Ruoslahti E. Hyaluronate binding properties of versican. J Biol Chem. 1992; 267:10003–10010. [PubMed: 1577773]

Ogawa Y, Schafer DP, Horresh I, Bar V, Hales K, Yang Y, Susuki K, Peles E, Stankewich MC, Rasband MN. Spectrins and ankyrinB constitute a specialized paranodal cytoskeleton. J Neurosci. 2006; 26:5230–5239. [PubMed: 16687515]

Oohashi T, Hirakawa S, Bekku Y, Rauch U, Zimmermann DR, Su WD, Ohtsuka A, Murakami T, Ninomiya Y. Bral1, a brain-specific link protein, colocalizing with the versican V2 isoform at the

nodes of Ranvier in developing and adult mouse central nervous systems. Mol Cell Neurosci. 2002; 19:43–57. [PubMed: 11817897]

Parkinson NJ, Olsson CL, Hallows JL, McKee-Johnson J, Keogh BP, Noben-Trauth K, Kujawa SG, Tempel BL. Mutant beta-spectrin 4 causes auditory and motor neuropathies in quivering mice. Nat Genet. 2001; 29:61–65. [PubMed: 11528393]

Pedraza L, Huang JK, Colman DR. Organizing principles of the axoglial apparatus. Neuron. 2001; 30:335–344. [PubMed: 11394997]

Pillai AM, Thaxton C, Pribisko AL, Cheng JG, Dupree JL, Bhat MA. Spatiotemporal ablation of myelinating glia-specific neurofascin (Nfasc NF155) in mice reveals gradual loss of paranodal axoglial junctions and concomitant disorganization of axonal domains. J Neurosci Res. 2009; 87:1773–1793. [PubMed: 19185024]

Poliak S, Gollan L, Salomon D, Berglund EO, Ohara R, Ranscht B, Peles E. Localization of Caspr2 in myelinated nerves depends on axon-glia interactions and the generation of barriers along the axon. J Neurosci. 2001; 21:7568–7575. [PubMed: 11567047]

Rasband MN. The axon initial segment and the maintenance of neuronal polarity. Nat Rev Neurosci. 2010; 11:552–562. [PubMed: 20631711]

Rasband MN, Peles E, Trimmer JS, Levinson SR, Lux SE, Shrager P. Dependence of nodal sodium channel clustering on paranodal axoglial contact in the developing CNS. J Neurosci. 1999; 19:7516–7528. [PubMed: 10460258]

Rios JC, Rubin M, St Martin M, Downey RT, Einheber S, Rosenbluth J, Levinson SR, Bhat M, Salzer JL. Paranodal interactions regulate expression of sodium channel subtypes and provide a diffusion barrier for the node of Ranvier. J Neurosci. 2003; 23:7001–7011. [PubMed: 12904461]

Saito T. In vivo electroporation in the embryonic mouse central nervous system. Nat Protoc. 2006; 1:1552–1558. [PubMed: 17406448]

Salzer JL. Polarized domains of myelinated axons. Neuron. 2003; 40:297–318. [PubMed: 14556710]

Schafer DP, Rasband MN. Glial regulation of the axonal membrane at nodes of Ranvier. Curr Opin Neurobiol. 2006; 16:508–514. [PubMed: 16945520]

Schafer DP, Bansal R, Hedstrom KL, Pfeiffer SE, Rasband MN. Does paranode formation and maintenance require partitioning of neurofascin 155 into lipid rafts? J Neurosci. 2004; 24:3176–3185. [PubMed: 15056697]

Schafer DP, Custer AW, Shrager P, Rasband MN. Early events in node of Ranvier formation during myelination and remyelination in the PNS. Neuron Glia Biol. 2006; 2:69–79. [PubMed: 16652168]

Seidl AH, Rubel EW, Harris DM. Mechanisms for adjusting interaural time differences to achieve binaural coincidence detection. J Neurosci. 2010; 30:70–80. [PubMed: 20053889]

Sherman DL, Tait S, Melrose S, Johnson R, Zonta B, Court FA, Macklin WB, Meek S, Smith AJ, Cottrell DF, Brophy PJ. Neurofascins are required to establish axonal domains for saltatory conduction. Neuron. 2005; 48:737–742. [PubMed: 16337912]

Susuki K, Rasband MN. Molecular mechanisms of node of Ranvier formation. Curr Opin Cell Biol. 2008; 20:616–623. [PubMed: 18929652]

Susuki K, Baba H, Tohyama K, Kanai K, Kuwabara S, Hirata K, Furukawa K, Furukawa K, Rasband MN, Yuki N. Gangliosides contribute to stability of paranodal junctions and ion channel clusters in myelinated nerve fibers. Glia. 2007; 55:746–757. [PubMed: 17352383]

Susuki K, Raphael AR, Ogawa Y, Stankewich MC, Peles E, Talbot WS, Rasband MN. Schwann cell spectrins modulate peripheral nerve myelination. Proc Natl Acad Sci USA. 2011; 108:8009–8014. [PubMed: 21518878]

Thaxton C, Pillai AM, Pribisko AL, Dupree JL, Bhat MA. Nodes of Ranvier act as barriers to restrict invasion of flanking paranodal domains in myelinated axons. Neuron. 2011; 69:244–257. [PubMed: 21262464]

Volkmer H, Zacharias U, Nörenberg U, Rathjen FG. Dissection of complex molecular interactions of neurofascin with axonin-1, F11, and tenascin-R, which promote attachment and neurite formation of tectal cells. J Cell Biol. 1998; 142:1083–1093. [PubMed: 9722619]

Yamaguchi Y. Lecticans: organizers of the brain extracellular matrix. Cell Mol Life Sci. 2000; 57:276–289. [PubMed: 10766023]

Yang Y, Lacas-Gervais S, Morest DK, Solimena M, Rasband MN. BetaIV spectrins are essential for membrane stability and the molecular organization of nodes of Ranvier. J Neurosci. 2004; 24:7230–7240. [PubMed: 15317849]

Yang Y, Ogawa Y, Hedstrom KL, Rasband MN. betaIV spectrin is recruited to axon initial segments and nodes of Ranvier by ankyrinG. J Cell Biol. 2007; 176:509–519. [PubMed: 17283186]

Zimmermann DR, Dours-Zimmermann MT. Extracellular matrix of the central nervous system: from neglect to challenge. Histochem Cell Biol. 2008; 130:635–653. [PubMed: 18696101]

Zonta B, Tait S, Melrose S, Anderson H, Harroch S, Higginson J, Sherman DL, Brophy PJ. Glial and neuronal isoforms of Neurofascin have distinct roles in the assembly of nodes of Ranvier in the central nervous system. J Cell Biol. 2008; 181:1169–1177. [PubMed: 18573915]

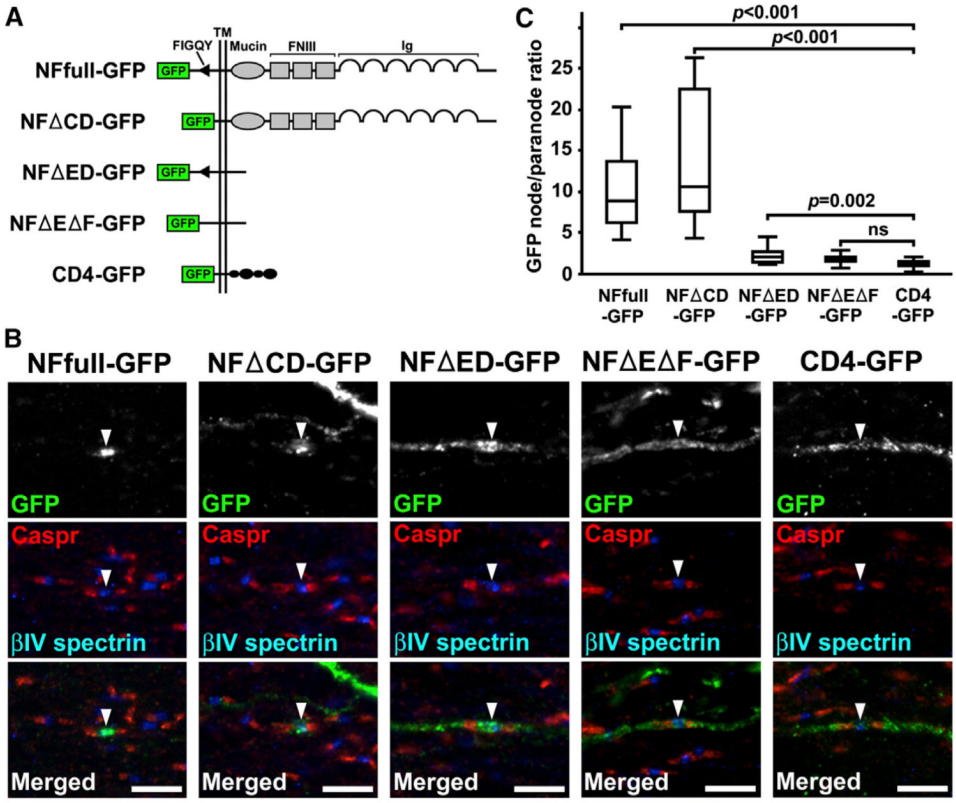

Figure 1. NF186 Can Cluster at Nodes through Extracellular or Cytoskeletal Interactions

(A) Cartoon showing the full-length and truncated constructs of NF186 and a membrane protein CD4 used in this experiment. FNIII, fibronectin type III domain; Ig, immunoglobulin domain.

(B) Coronal sections of electroporated mouse brains immunostained for GFP (green), Caspr (red), and βIV spectrin (blue). Arrowheads indicate nodes of Ranvier. Scale bars, 5 μm.

(C) The node/paranode ratio of GFP signals in the axons introduced with NFfull-GFP (n = 14), NFΔCD-GFP (n = 10), NFΔED-GFP (n = 14), NFΔEΔF-GFP (n = 16), or CD4-GFP (n = 18). Data were collected from two brains in each group.

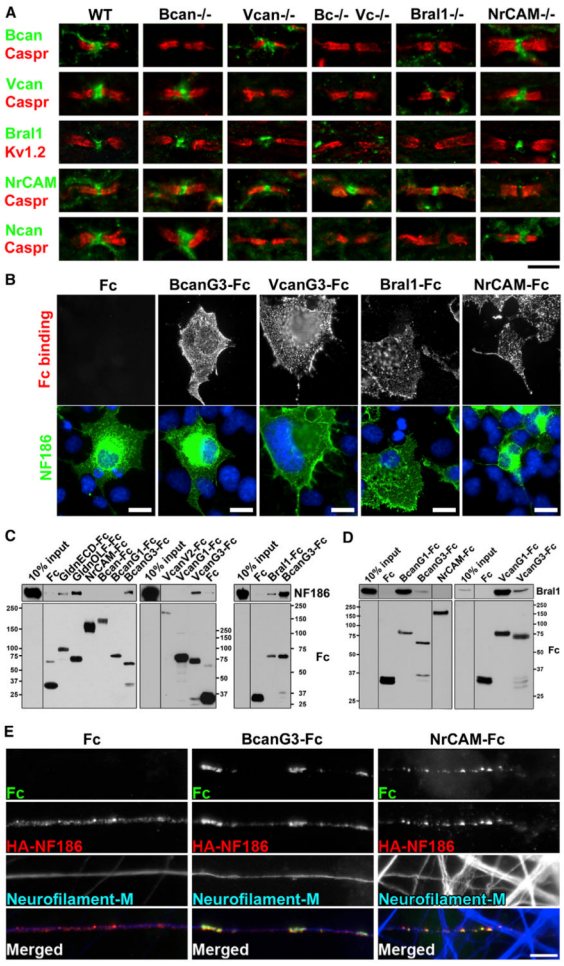

Figure 2. Node-Enriched ECM Components Interact with and Cluster NF186

(A) Adult WT and mutant mouse spinal cord immunostained using antibodies against various ECM components (green) and the paranodal marker Caspr (red) or the juxtaparanodal marker Kv1.2 (red). Scale bar, 10 mm for Bral1 staining and5 mm for all the others.

(B) Fc fusion proteins of BcanG3, VcanG3, NrCAM, and Bral1 bind to COS-7 cells transfected withHA-NF186 (green). Fc alone was used as a negative control. Cell nuclei were visualized by Hoechstin blue. Scale bars = 20 μm.

(C) Pull-down analysis shows binding between BcanG3, VcanG3, or Bral1 and the secreted NF186 extracellular domain. GldnECD is the whole extracellular domain of gliomedin, and GldnOLF is the olfactomedin domain of gliomedin; both serve as positive controls. Molecular weight markers in kDa.

(D) Pull-down analysis shows binding between BcanG1 or VcanG1 and Bral1.

(E) Clustering of BcanG3-Fc or NrCAM-Fc (green) and HA-NF186 (red) along axons (visualized by anti-neurofilament-M) of cultured DRG neurons. Scale bar, 5 μm.

See also Figure S1 and Table S1.

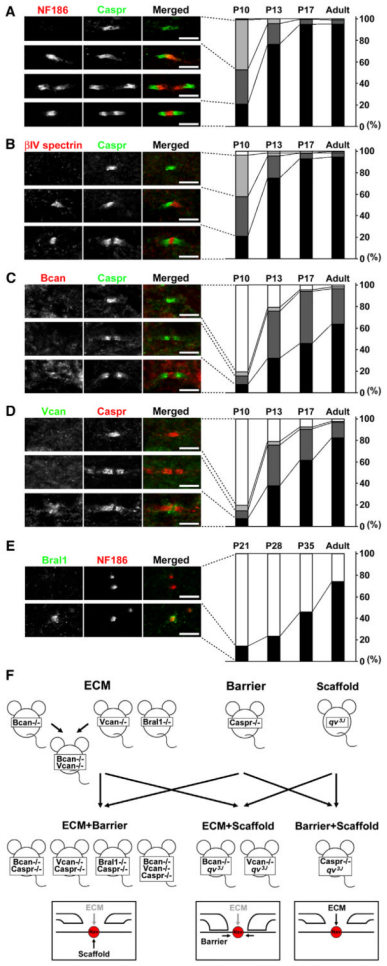

Figure 3. Developmental Clustering of Nodal and Paranodal Components in the CNS

(A–E) Rat optic nerve sections were immunostained with antibodies to nodal or paranodal markers as indicated in the left panels showing representative images of different stages of CNS node formation. Scale bars, 5 μm. Right panels show a quantitative analysis of each type of staining as a function of age. The data were obtained by observation of 200–250 sites from two animals at each time point indicated.

(F) Schematic of the genetic strategy used to test whether multiple mechanisms contribute to CNS node of Ranvier formation. ECM mutants, PJ mutants (barrier), and CS mutants (scaffold) were crossed to generate double- or triple-mutant mice with two mechanisms disrupted simultaneously. (N.B. The core ECM molecules at the CNS nodes cannot be completely removed in ECM+Barrier or ECM+Scaffold mutant mice.)

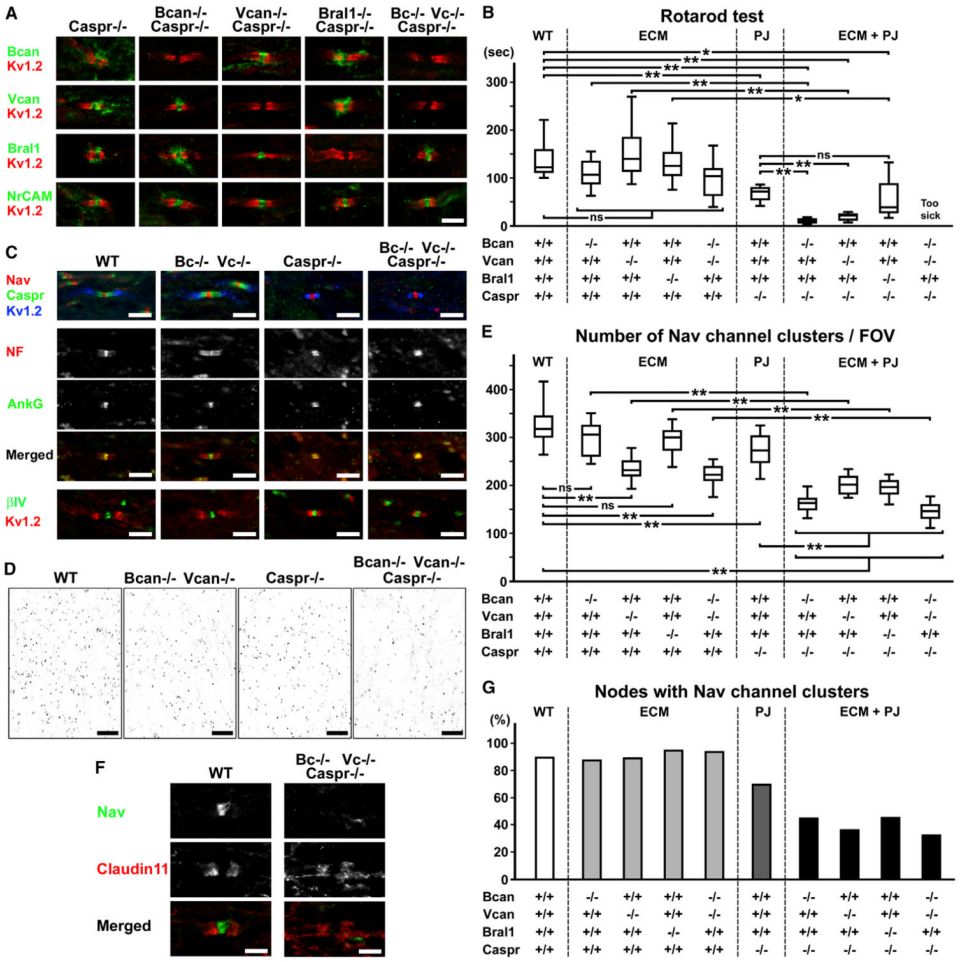

Figure 4. Mutant Mice with Disrupted CNS Nodal ECM and Paranodes

(A) Loss of ECM molecules in the mutants at P18. Spinal cord sections were stained as indicated. Kv1.2 channels were mislocalized to paranodes due to the loss of Caspr. Scale bar, 5 μm for all panels.

(B) Accelerating rotarod test performed at P18.

(C) Representative images of nodal and paranodal components. P18 optic nerve sections were immunostained as indicated. Note that the Kv1.2 channels (blue) are mislocalized to paranodes in Caspr-deficient mutants.

(D) Na^+ channel staining at nodes of Ranvier (black dots) in the optic nerves of the indicated mutant mice at P18. Scale bars, 20 μm.

(E) Quantitation of the number of Na^+ channel clusters per field of view (FOV, depicted in D). Data are collected from 20 FOVs from two animals.

(F) P18 spinal cord nodes of Ranvier immunostained using antibodies against Na^+ channels (Nav; green) and claudin-11 (red).

(G) Frequency of Na^+ channel clusters at nodes. More than 200 nodes (defined by two claudin-11-labeled paranodes) were observed in spinal cords from two animals in each group.

ECM, mutant mice lacking one or two ECM molecules; PJ, $Caspr^{-/-}$ mice lacking PJs. *$p < 0.01$, **$p < 0.001$; ns, not significant. See also Figure S2 and Movie S1.

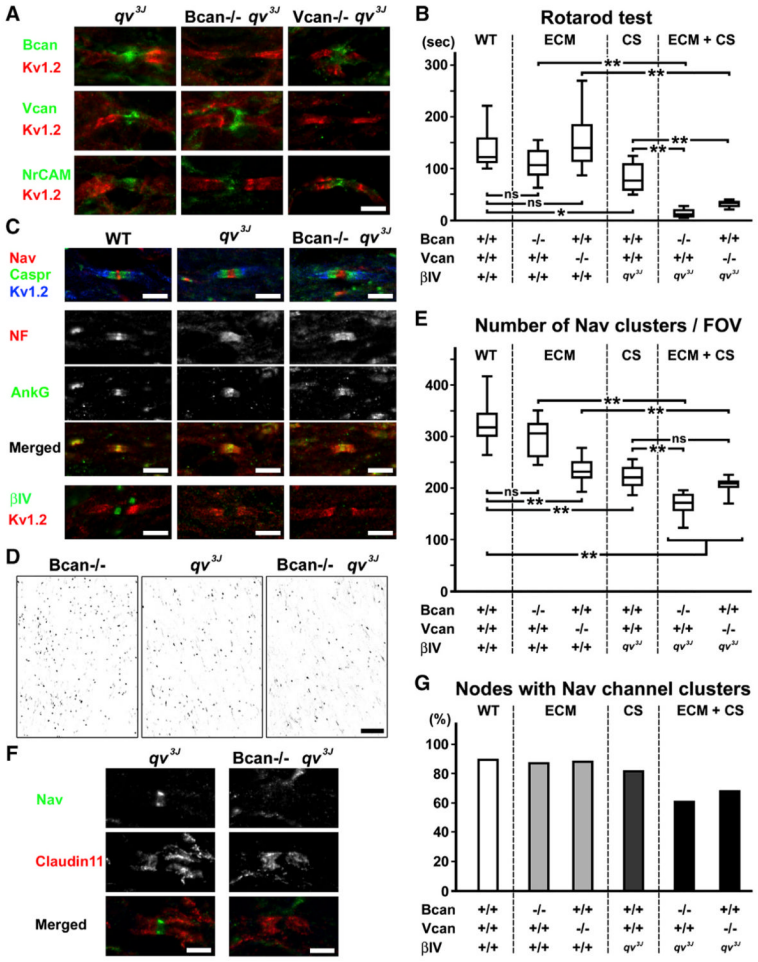

Figure 5. Mutant Mice with Disrupted CNS Nodal ECM and Nodal Cytoskeleton

(A) Loss of ECM molecules in the indicatedmutants at P18. Spinal cord sections were stained as indicated. Scale bar, 5 μm for all panels.

(B) Accelerating rotarod test performed at P18.

(C) Representative images of nodal and paranodal components. P18 optic nerve sections were immunostained as indicated. Note the loss of βIV spectrin in Bcan$^{-/-}$ *qv3J* double mutants.

(D) Na^+ channel staining at nodes of Ranvier (black dots) in the optic nerves of the indicated mutant mice at P18. The density of Na^+ channel clusters is reduced in Bcan$^{-/-}$ *qv3J* double mutants. Scale bars, 20 μm.

(E) Quantitation of the number of Na^+ channel clusters per FOV (depicted in D). Data were collected from 20 FOVs from two animals in each group.

(F) P18 spinal cord nodes of Ranvier immunostained using antibodies against Na^+ channels (Nav; green) and claudin-11 (red).

(G) Frequency of Na^+ channel clusters at nodes. More than 200 nodes (defined by two claudin-11-labeled paranodes) were observed in spinal cords from two animals in each group.

ECM, mutant mice lacking a single ECM molecule; CS, *qv3J* mice lacking nodal βIV spectrin. *p < 0.01, **p < 0.001; ns, not significant. See also Figure S3 and Movie S2.

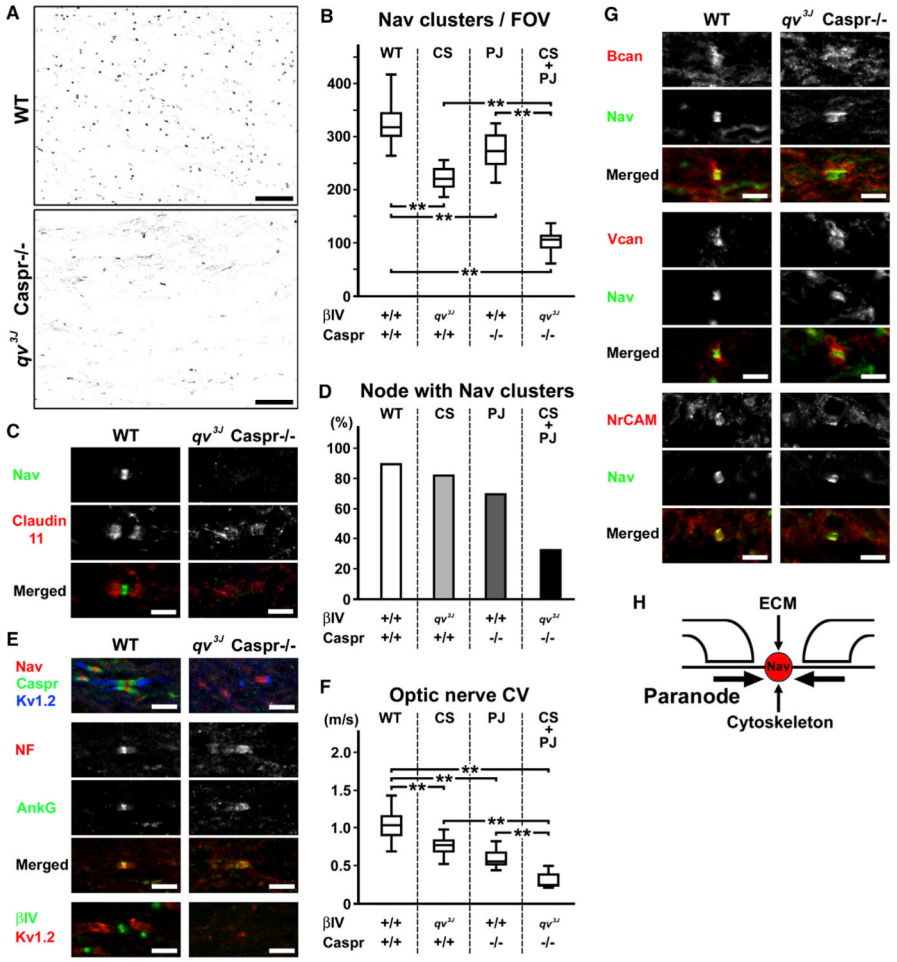

Figure 6. CNS Nodes Are Dramatically Disrupted in Mutant Mice Lacking Paranodes and the Nodal Cytoskeleton

(A) Na^+ channel staining in the optic nerves at P18. The density of Na^+ channel clusters (black dots) is dramatically reduced in *qv3J* Caspr$^{-/-}$ mice. Scale bars, 20 μm).

(B) Quantitation of the number of Na^+ channel clusters in the optic nerves at P18 per FOV (depicted in A). Data were collected from 20 FOVs from two animals in each group.

(C) P18 spinal cord nodes of Ranvier immunostained using antibodies against Na^+ channels (Nav; green) and claudin-11 (red).

(D) The frequency of Na^+ channel clusters at nodes. More than 200 nodes (defined by two claudin-11-labeled paranodes) were observed in spinal cords from two animals in each group.

(E) Immunostaining of P18 optic nerve sections shows disorganized nodal and juxtaparanodal domains in *qv3J* Caspr$^{-/-}$ mice. Optic nerves were labeled as indicated. Scale bars = 5 μm.

(F) Optic nerve CAP conduction velocities. Significant slowing was observed in *qv3J* Caspr$^{-/-}$ mice compared with WT, *qv3J*, or Caspr$^{-/-}$ mice. The analyses were performed at P17 or P18.

(G) Localization of ECM molecules surrounding Na^+ channel clusters. Spinal cord sections at P18 were stained as indicated. Scale bars, 5 μm.

(H) Cartoon showing three mechanisms involved in CNS node formation. The primary mechanism in the CNS is the paranodal barrier mechanism. PJ, Caspr$^{-/-}$ mice lacking PJs;

CS, *qv3J* mice lacking nodal βIV spectrin. **p < 0.001; ns, not significant. See also Figure S4 and Movie S3.

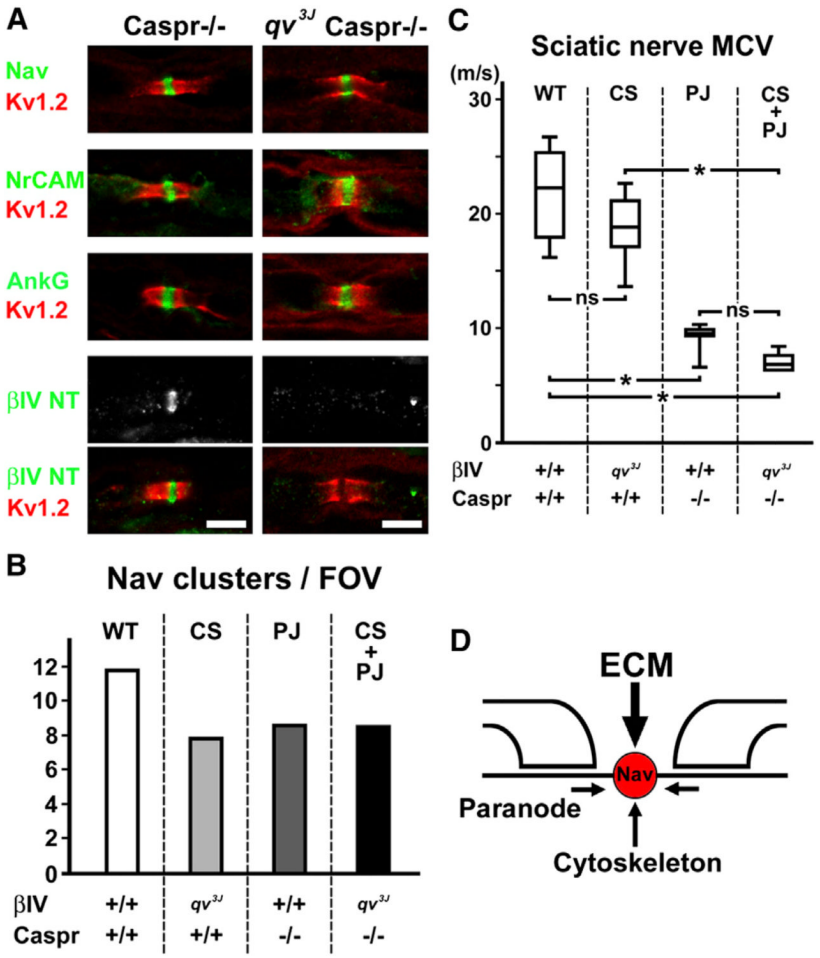

Figure 7. PNS Nodes Form Properly in Mutant Animals with Disrupted Paranodes and Axonal Cytoskeleton

(A) Sciatic nerve sections at P18 were stained as indicated. Nodal organization is preserved in the PNS of *qv3J* Caspr$^{-/-}$ mice. Scale bars = 5 μm.

(B) Quantitation of the number of Na^+ channel clusters in the sciatic nerves at P18 per FOV. Bars indicate the mean value of ~25 FOVs from two animals in each group.

(C) Motor nerve conduction velocity in sciatic nerves at P18. No significant difference was seen between Caspr$^{-/-}$ and *qv3J* Caspr$^{-/-}$ mice. *$p < 0.01$; ns, not significant.

(D) Cartoon showing three mechanisms involved in PNS node formation. Among these three mechanisms, the primary one is the ECM mechanism. PJ, Caspr$^{-/-}$ mice lacking PJs; CS, *qv3J* mice lacking nodal βIV spectrin.